Article

Long-Term Stability Test for Femtosecond Laser-Irradiated SnO$_2$-Nanowire Gas Sensor for C$_7$H$_8$ Gas Sensing

Sanghoon Ahn [1],[†] , **Kang Woo Chun [2],[†]** and **Changkyoo Park [3],***

[1] Laser and Electron Beam Application Department, Korea Institute of Machinery and Materials, Daejeon 34103, Republic of Korea; shahn@kimm.re.kr
[2] Division of Marine System Engineering, National Korea Maritime & Ocean University, Busan 49112, Republic of Korea; kwchun@kmou.ac.kr
[3] Department of Materials Science and Engineering, Seoul National University of Science and Technology, Seoul 01811, Republic of Korea
[*] Correspondence: ck0421@seoultech.ac.kr
[†] These authors contributed equally to this work.

Abstract: In this study, femtosecond (FS) laser irradiation with different laser energy densities of 138, 276, and 414 mJ/cm^2 is applied to SnO$_2$-nanowire (NW) gas sensors, and the effect of the FS laser irradiation on the gas sensor response toward toluene (C$_7$H$_8$) gas is investigated. The FS laser irradiation causes oxygen deficiency in the SnO$_2$ NWs and forms SnO and SnO$_x$. Moreover, an embossing surface with multiple nano-sized bumps is created on the SnO$_2$ NW surface because of the FS laser irradiation. The FS laser-irradiated SnO$_2$-NW gas sensor exhibits superior sensing performance compared with the pristine SnO$_2$-NW gas sensor. Moreover, the FS laser energy density significantly affects gas-sensing performance, and the highest sensor response is achieved by the gas sensor irradiated at 138 mJ/cm^2. The long-term stability test of the laser-irradiated SnO$_2$-NW gas sensor is performed by comparing fresh and 6-month-old gas sensors in different gas concentrations and relative humidity levels. Comparable gas-sensing behaviors are examined between the fresh and 6-month-old gas sensor, and this verifies the robustness of the laser-irradiated SnO$_2$-NW gas sensor.

Keywords: femtosecond laser irradiation; SnO$_2$ nanowire; gas sensor; C$_7$H$_8$ gas; long-term stability

1. Introduction

Gas sensors have been widely used to protect the environment and human health as well as to control production quality in industrial applications [1,2]. Semiconducting metal oxide (SMO) gas sensors are one of the most widely used gas sensors because of their low cost, rapid response, and excellent sensitivity and stability [3]. Toluene (C$_7$H$_8$) is a well-known volatile organic compound (VOC) released from various household products such as flooring, furniture, and paintings. Therefore, we are repeatedly exposed to C$_7$H$_8$ environments, which can cause short- and long-term health risks, including throat, nose, and eye irritation, as well as liver and kidney cancers [4]. Therefore, to protect public health, the performance of SMO gas sensors should be further improved for an accurate and rapid examination of C$_7$H$_8$.

Various strategies have been investigated to improve the sensing capabilities of SMO gas sensors, including heterojunction formation [5,6], noble-metal functionalization [7], doping [8], surface engineering [9,10], and irradiation [11–19]. Surface engineering focuses on enlarging the surface area to improve the sensing performance via the formation of one-, two-, or three-dimensional nanomaterials or the generation of surface roughness on the surface of the sensing material [9,10]. Irradiation techniques, including gamma-ray irradiation [15], plasma treatment [12], ion implantation [16], electron-beam irradiation [13,14], and laser irradiation [17,20,21], are another approach for improving sensing performance.

Applying external energy to sensing materials via irradiation induces structural defects (e.g., oxygen deficiency), and the associated non-stoichiometry contributes to increased interaction with gases. Therefore, non-stoichiometric metal oxides offer improved sensing performance [20]. Among the irradiation techniques, laser irradiation is promising owing to its ease of control, rapid and precise process, and no requirement for a clean room or vacuum chamber. Hou et al. [18] reported that pulsed laser irradiation improved the response of an Al-doped ZnO gas sensor toward H_2 gas. Moreover, Zhang et al. [19] applied an excimer laser to a WO_3 gas sensor and demonstrated improved performance toward NO_2 gas.

Among the various SMO gas sensors, SnO_2 is a promising sensing material owing to its excellent stability, high electron mobility, non-toxicity, and low synthesis cost [21]. The different morphologies of SnO_2 include nanoneedles, nanofibers, films, nanoparticles, nanowires, and hollow spheres [22–29]. SnO_2 nanowires have been widely adopted as a sensing material owing to their large surface areas, which enables more target gases to be absorbed, thus resulting in better sensing response [27–29]. However, the sensing performance should be enhanced to accurately examine the presence of C_7H_8.

In this study, the femtosecond (FS) laser is irradiated on the SnO_2 NWs, and the effect on the gas-sensing behavior of the NWs is investigated. Different laser energy densities are applied to the SnO_2 NWs, and the sensing behaviors of the pristine and laser-irradiated SnO_2 NWs toward C_7H_8 are examined. The laser-irradiated SnO_2 NWs perform better in terms of gas-sensing behavior compared with that of the pristine SnO_2 NWs. Therefore, transmission electron microscopy (TEM) and electron energy loss spectroscopy (EELS) are performed to determine the changes in the surface morphology and chemical state of the SnO_2 NWs after the FS laser irradiation. The FS laser irradiation increases the surface area and results in structural defects in the SnO_2 NWs, which are characteristic of surface engineering and irradiation techniques. The results of this study verify that the ultrashort pulse laser irradiation is a promising approach for enhancing the sensing capability of SnO_2 NWs.

2. Experimental

2.1. Synthesis of SnO₂ NWs

An Au-catalyzed vapor–liquid–solid (VLS) technique was adopted for the SnO_2 NWs' growth. Details regarding the VLS technique are available in our previous paper [30]. A Si wafer with a SiO_2 layer (thickness: 200 nm) was utilized as the substrate. Tri-layered electrodes comprising Ti (50 nm), Pt (200 nm), and Au (3 nm) were deposited onto the substrate via sputtering. A tri-layer-deposited substrate with metallic Sn powder (99.9%, Sigma-Aldrich, St. Louis, MO, USA) was placed in a quartz tube furnace. The furnace was heated up to 900 °C under a gas flow comprising N_2 (300 sccm) and O_2 (10 sccm). Thus, a SnO_2 NW-based gas sensor device was fabricated. Figure 1 shows a field emission scanning electron microscopy (FE-SEM) image of a successfully grown network of SnO_2 NWs on tri-layered electrodes.
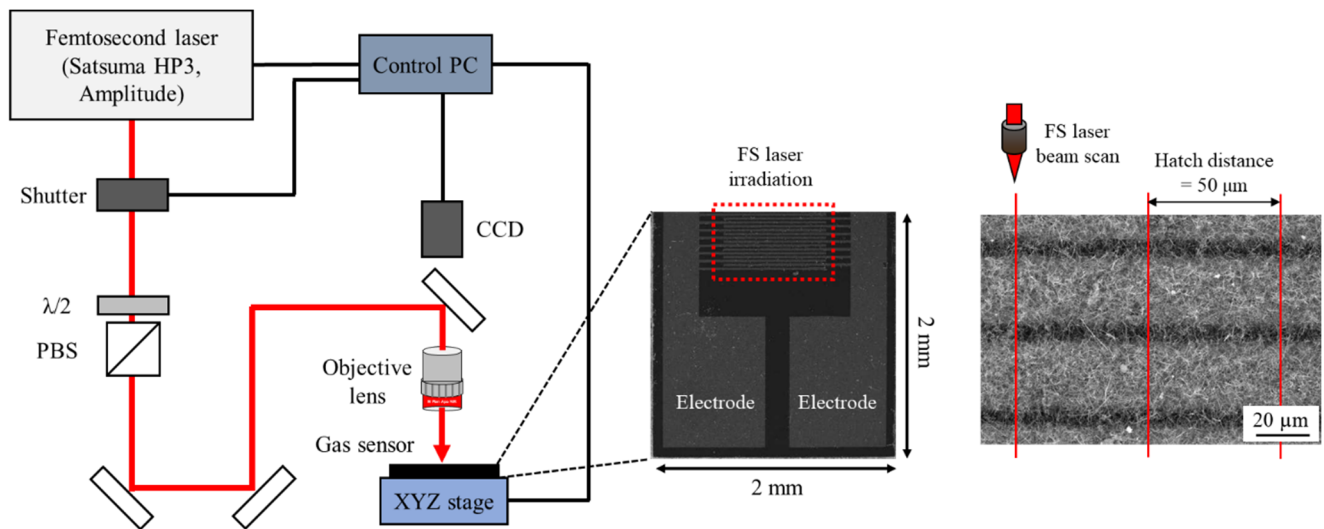
Figure 1. Schematic diagrams of laser system, gas sensor electrode, and FS laser-irradiation procedure.

2.2. Femtosecond Laser Irradiation

The experimental setup for the FS laser irradiation is shown in Figure 1. An FS laser (Satsuma HP³, Amplitude Laser, Pessac, France) with a central wavelength of 1030 nm, pulse duration of 350 fs, and frequency of 15 kHz was applied to the gas sensor device. The laser beam quality (M^2) was measured to be 1.2 in both the horizontal and vertical directions. The laser pulse energy was controlled using a half-wave plate and thin-film polarizing beam splitter (PBS) combined, and the laser beam was delivered by a beam mirror train. The laser beam was focused on the gas sensor device through a $10\times$ infinity corrected microscope objective lens, thus resulting in a laser beam diameter of 4.8 μm. The laser beam scanning speed was set to 80 mm/s using a computer-controlled motion system (M-414, PI Benelux, Karlsruhe, Germany). The FS laser was irradiated on a network of SnO_2 NWs (at the dotted red region in the gas sensor device, as shown in Figure 1) at a hatch distance of 50 μm. Fifteen linear laser-beam scans were performed. The applied laser pulse energies were 0.025, 0.05, and 0.075 μJ, which were equivalent to the laser fluences of 138, 276, and 414 mJ/cm^2, respectively. The laser fluence was calculated as follows:

$$\text{Laser fluence (mJ/cm}^2) = \text{Laser pulse energy (mJ)/Laser beam area (cm}^2) \qquad (1)$$

2.3. Characterization

A qualitative analysis of the SnO_2 NWs was conducted via X-ray diffraction (XRD, X'Pert PRO, PANalytical, Malvern, UK) using Cu-Ka radiation (λ = 1.5418 Å). The morphology and microstructure of the SnO_2 NWs was examined via FE-SEM (Hitachi S-4200, Tokyo, Japan) and transmission electron microscopy (TEM, Carl Zeiss LIBRA 200 MC, Jena, Germany). The fabricated SnO_2 NWs were dispersed in isopropyl alcohol and deposited onto a Cu TEM grid (01890-F, Ted Pella, Inc., Redding, CA, USA) to prepare the TEM specimens. The electron energy loss spectroscopy (EELS) analysis was conducted to examine the chemical characteristics of the pristine and laser-irradiated SnO_2 NWs. The first O peak in the EELS spectra (at approximately 532 eV) was used as a reference to align the EELS spectra of the pristine and laser-irradiated SnO_2 NWs. Subsequently, peak analysis was conducted [31].

2.4. Gas-Sensing Measurements

A customized gas-sensing system was adopted to examine the gas-sensing behavior. A gas chamber was placed in a quartz tube furnace, and the operating temperature of the gas sensor was controlled. The concentration of the target gas (C_7H_8 gas in this study)

was determined by mixing it with dry air, and the gas mixing ratio was controlled using mass-flow controllers. The mixture was flowed at 500 sccm.

The gas-sensing behavior was measured using a custom-developed gas-sensing system. The gas chamber was placed in a quartz tube furnace to control the operating temperature of the gas sensor. The target gas was mixed with dry air using mass-flow controllers to obtain its specific gas concentrations. The flow rate was maintained at 500 sccm. A Keithley source meter (Series 2400) was used to measure the electrical resistance during the sensing measurements in air (R_a) and target gas (R_g) atmospheres, and the sensor response was calculated as $R = R_g/R_a$. Moreover, the response time (τ_{res}) was measured at the time for the sensor to reach 90% of its final resistance value after supplying the target gas, whereas the recovery time (τ_{res}) was measured at the time for the sensor to reach 90% of its initial resistance value after the target gas supply was halted. To investigate the effect of humidity, we examined the sensing behavior at different relative humidity (RH) values. The long-term stability tests were conducted by comparing the fresh and 6-month-old gas sensors in various target gas concentrations and RH values.

3. Results and Discussions

3.1. Microstructures

Figure 2 shows the qualitative XRD analysis of the pristine SnO_2 NWs (Figure 2a) and laser-irradiated SnO_2 NWs with different laser energy densities of 138 (Figure 2b) and 414 (Figure 2c) mJ/cm^2. For each specimen, the XRD patterns were consistent with those of crystalline SnO_2 (tetragonal rutile structure, JCPDS File No. 88-0287 [32]), and no additional peaks were observed. Figure 3a,b shows the TEM images of the pristine SnO_2 NW and laser-irradiated SnO_2 NW with a laser energy density of 138 mJ/cm^2, respectively. High-resolution TEM images and selected area electron diffraction (SAED) patterns are shown in red boxes. For the pristine SnO_2 NW, a smooth and flat nanowire surface was observed. Moreover, both the d-spacing and SAED pattern analyses verified the tetragonal rutile structure of the SnO_2 NWs [33]. For the laser-irradiated SnO_2 NW, the equivalent crystal structure was analyzed based on the d-spacing and SAED pattern, which indicated no crystal structure change after the FS laser irradiation. However, multiple FS laser irradiation-induced nano-sized bumps developed on the nanowire surface (denoted by red arrows). This embossing surface may create more adsorption sites for gas species, thus improving sensing performance.

The EELS analysis was performed to determine the chemical states before and after the FS laser irradiation. Figure 4 shows the energy-loss spectra of the pristine SnO_2 NWs and laser-irradiated SnO_2 NWs with a laser energy density of 138 mJ/cm^2. According to Moreno et al. [31], the EELS spectrum can be used to identify different Sn oxides (i.e., SnO_2, SnO, and SnO_x); thus, in this study, the EELS spectra before and after the FS laser irradiation were used to examine the chemical state of Sn oxides. For the pristine SnO_2 NWs, the EELS spectrum was equivalent to that reported by Moreno et al. [31]. The O K-edge in the energy range of 527–545 eV comprised two peaks, and the peak separation was 5.82 eV. Moreover, the Sn $M_{4,5}$ edges in the energy range of 490–505 eV and single distinct Sn M_4 and M_5 edges were examined at 495.83 and 501.26 eV, respectively. However, a slightly different EELS spectrum was observed for the laser-irradiated SnO_2 NWs with respect to the peak shifts and generations. A relatively large peak separation (6.25 eV) was detected at the O K-edge, and multiple Sn $M_{4,5}$ edges were observed at the Sn M edge. These modifications in the EELS spectrum contributed to the formation of SnO or SnO_x phases after the FS laser irradiation. The SnO_2 and SnO have different peak positions at the O K edge and Sn $M_{4,5}$ edges [31]. Consequently, the presence of SnO or SnO_x (developed from a combination of SnO_2 and SnO) in SnO_2 resulted in a slightly larger O K edge separation and multiple Sn $M_{4,5}$ edges, thus indicating that the presence of different Sn oxides (i.e., SnO_2, SnO, and SnO_x) was caused by the FS laser irradiation.
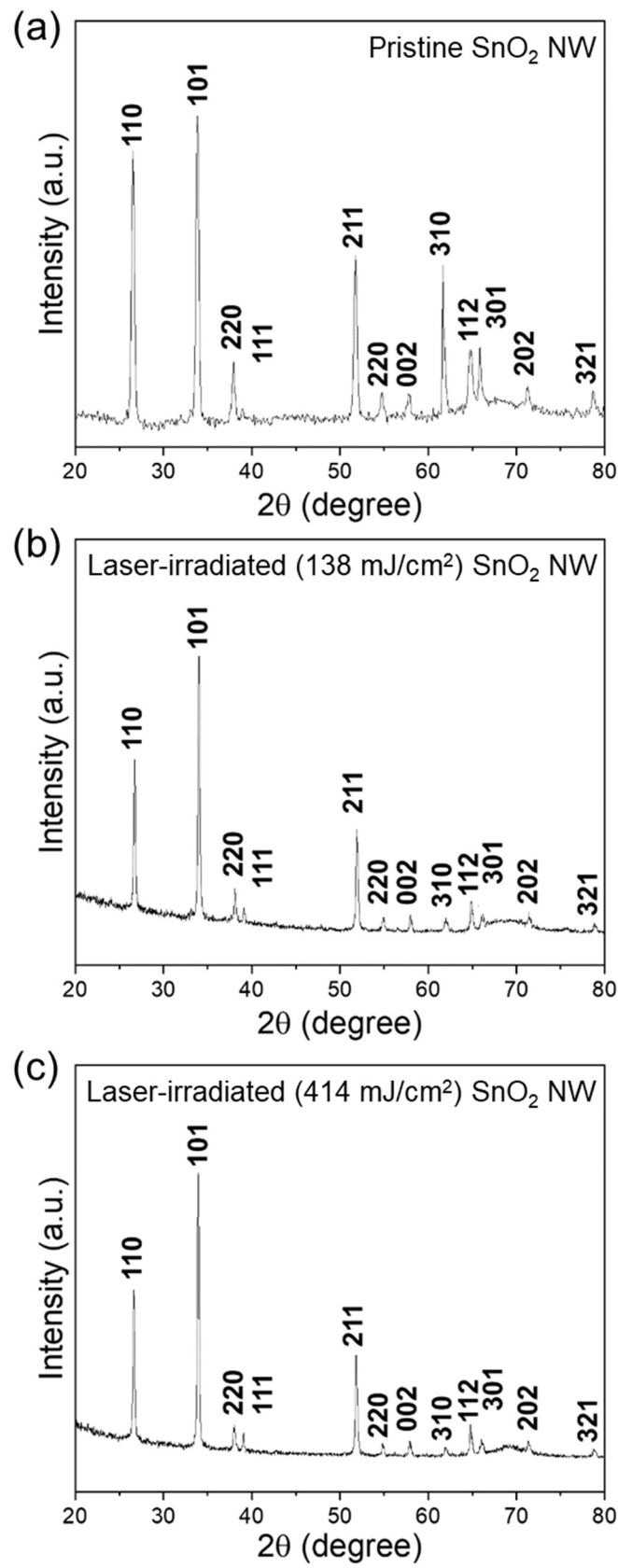
Figure 2. XRD spectra for the (**a**) pristine SnO_2 NW, (**b**) laser-irradiated SnO_2 NW with a laser energy density of 138 mJ/cm^2, and (**c**) laser-irradiated SnO_2 NW with a laser energy density of 414 mJ/cm^2.
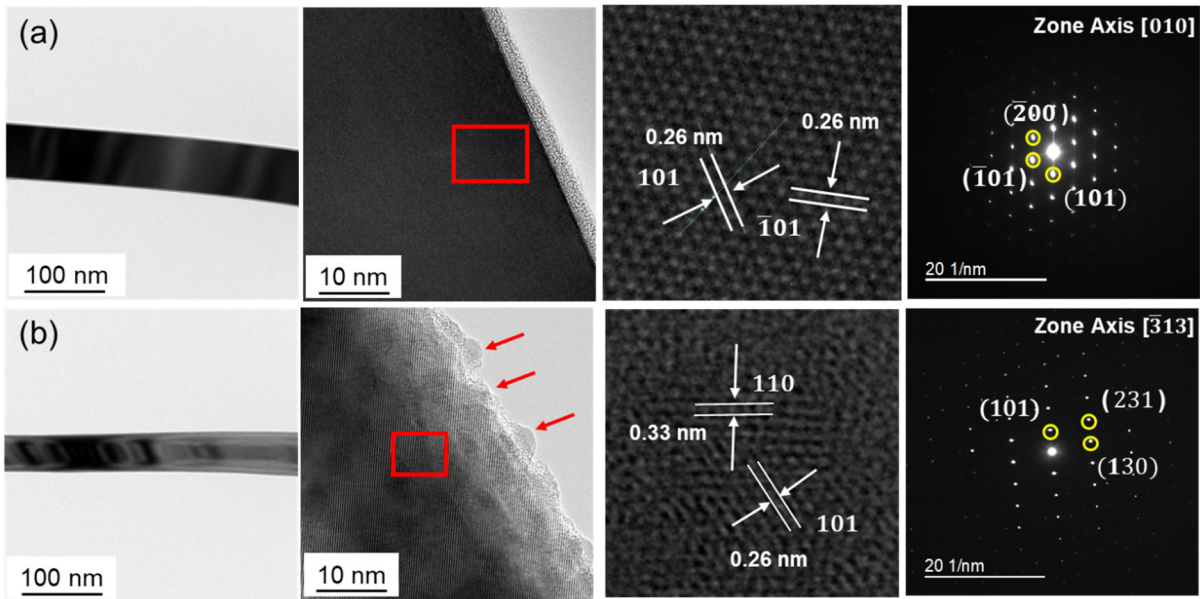
Figure 3. TEM image, high-resolution TEM image, and SAED pattern of the (**a**) pristine SnO_2 NW and (**b**) laser-irradiated SnO_2 NW with a laser energy density of 138 mJ/cm².
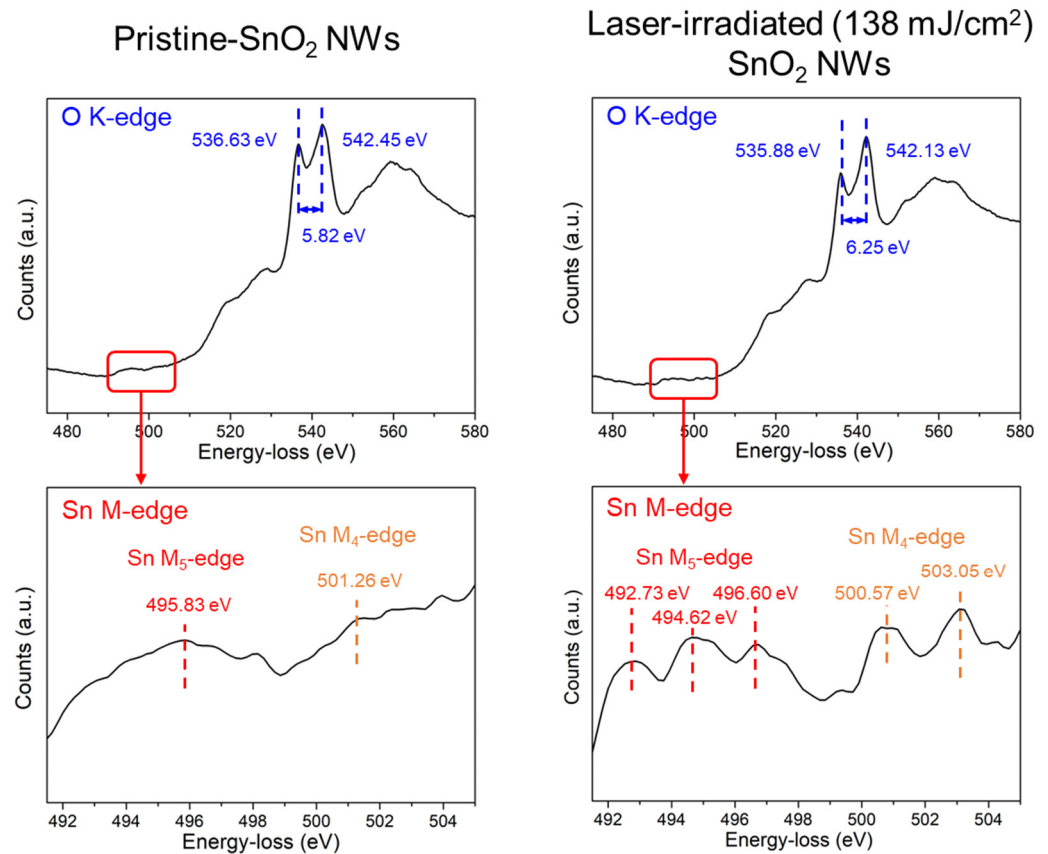

Figure 4. EELS spectra of O K edge and Sn $M_{4,5}$ edges for the pristine SnO_2 NW and laser-irradiated SnO_2 NW with a laser energy density of 138 mJ/cm².

3.2. Gas-Sensing Studies

Figure 5a shows the transient resistance curves of the pristine gas sensor in the range of 50–350 °C for 10, 30, and 50 ppm of C_7H_8 gas, and the corresponding sensor response and base resistance are shown in Figure 5b. At 50 °C, no response was observed, whereas marginal resistance changes were indicated at 100 °C once the target gas supply was

introduced and halted. The resistance decreased slightly as the target gas supply was introduced, which is characteristic of the gas-sensing behavior of n-type SMO gas sensors. As the temperature increases, more significant resistance changes and higher sensor responses were observed. Moreover, the optimum sensing performance was observed at 300 °C, where the sensor indicated a response level of 1.52 at 50 ppm of C_7H_8 gas. Meanwhile, the resistance change and sensor response observed at 350 °C were lower than those observed at 300 °C. No gas sensor response was indicated at low temperatures because the target gas molecules did not possess sufficient energy to overcome the adsorption barrier. At 300 °C, the desorption rate of the oxygen molecules and the absorption rate of the target molecules were equivalent, thus resulting in the optimum sensing performance. At 350 °C, the desorption rate exceeded the adsorption rate; therefore, a relatively weaker sensor response was achieved compared with that achieved at 300 °C. Thus, subsequent gas-sensing tests were performed at 300 °C.
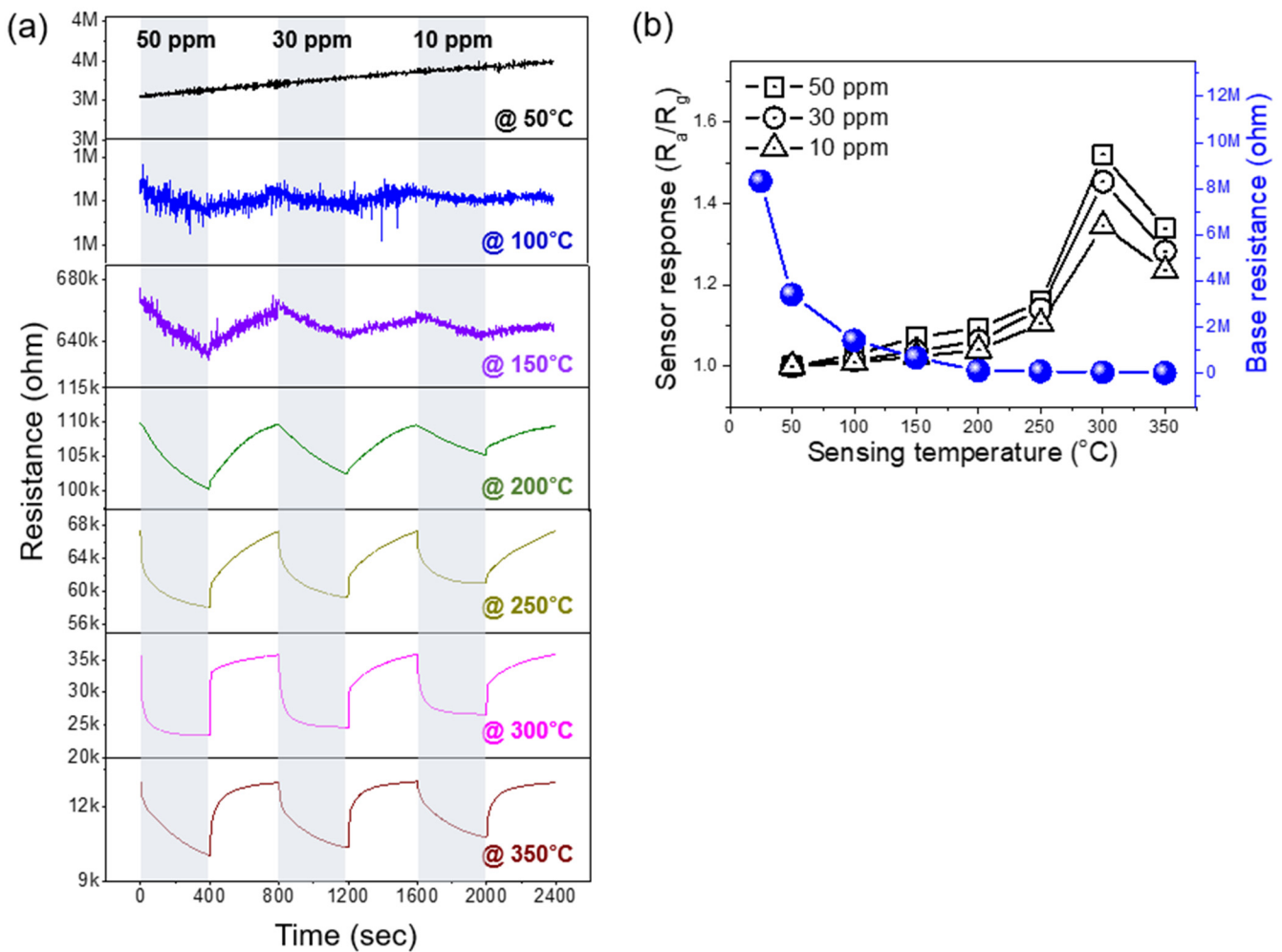

Figure 5. (**a**) Dynamic resistance curves of the pristine SnO_2 NWs for 10, 30, and 50 ppm of C_7H_8 gas at different sensing temperatures. (**b**) Corresponding sensor response and base resistance as a function of sensing temperature.

Figure 6a shows the dynamic resistance curves of the pristine SnO_2 NWs and laser-irradiated SnO_2 NWs with the laser energy densities of 138, 256, and 414 mJ/cm^2 toward 10, 30, and 50 ppm of C_7H_8 gas. Figure 6b shows the corresponding sensor response and base resistance as a function of the laser energy density. The sensor response for the pristine SnO_2 NWs was 1.52 at 50 ppm of C_7H_8 gas, whereas that for the laser-irradiated SnO_2 NWs with a laser energy density of 138 mJ/cm^2 was 2.42. The sensor response decreased as the laser energy density increased; interestingly, the sensor with higher base resistance

values exhibited better sensor response toward C_7H_8 gas. Figure 6c shows the response and recovery times as a function of the laser energy density toward 50 ppm of C_7H_8 gas. The shortest response and recovery times were indicated by the laser-irradiated SnO_2 NWs with a laser energy density of 138 mJ/cm^2, which demonstrated the highest sensor response. This result verifies that the FS laser irradiation improves the gas-sensing performance, and laser parameters significantly affect the gas-sensing performance.
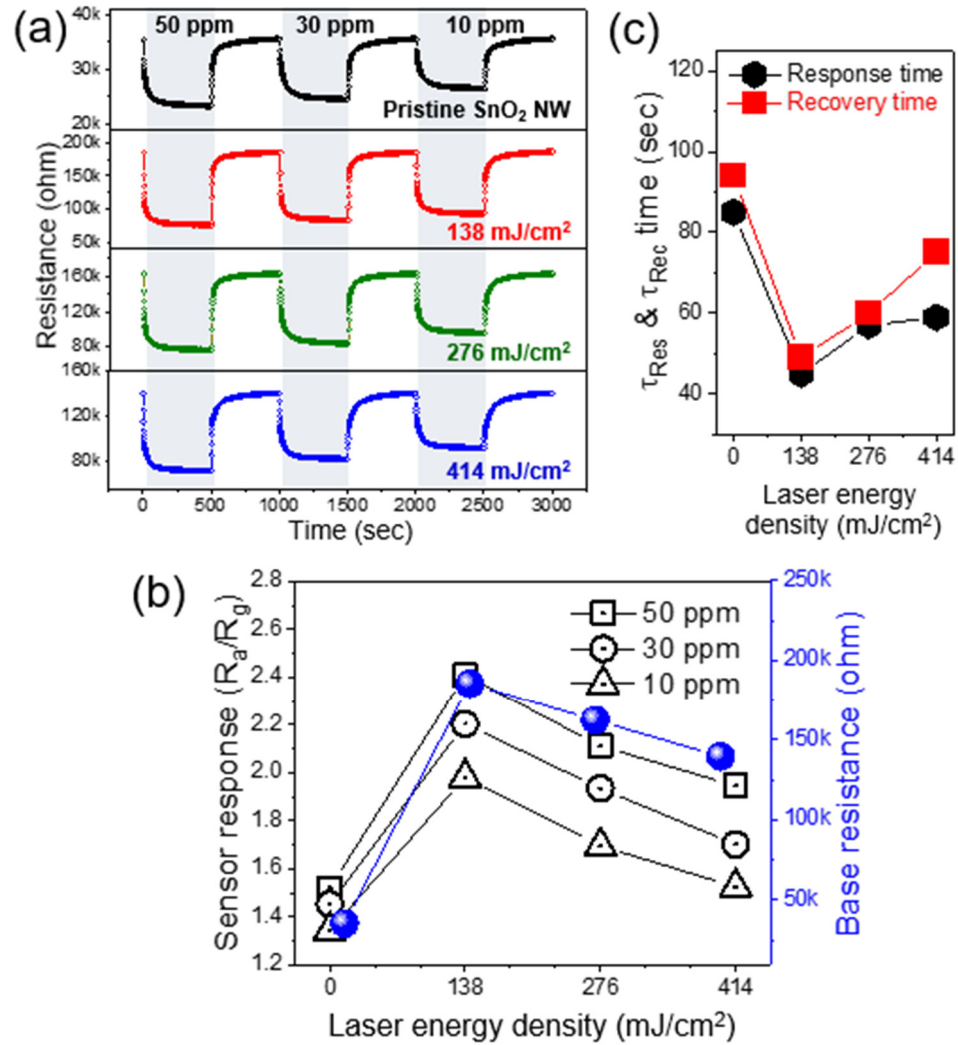

Figure 6. (**a**) Dynamic resistance curves of the pristine and laser-irradiated SnO_2 NWs (laser energy density: 138, 276, and 414 mJ/cm^2) for 10, 30, and 50 ppm of C_7H_8 gas. (**b**) Corresponding sensor response and base resistance as a function of laser energy density. (**c**) Corresponding response and recovery times as a function of laser energy density toward 50 ppm of C_7H_8 gas.

Gas-sensing tests were conducted at different RH values to examine the reliability of the SnO_2 gas sensor. Figure 7 shows the dynamic resistance curves and the corresponding sensor response and base resistance for the pristine SnO_2 NWs (Figure 7a) and laser-irradiated SnO_2 NWs with a laser energy density of 138 mJ/cm^2 (Figure 7b) toward 10, 30, and 50 ppm of C_7H_8 gas. Both gas sensors showed deteriorated sensing performance as the RH level increased. This is because water molecules may adhere to the adsorption sites of the SnO_2 NWs, where the target gas should be adsorbed, thus deteriorating the sensing performance as the RH level increases [34].
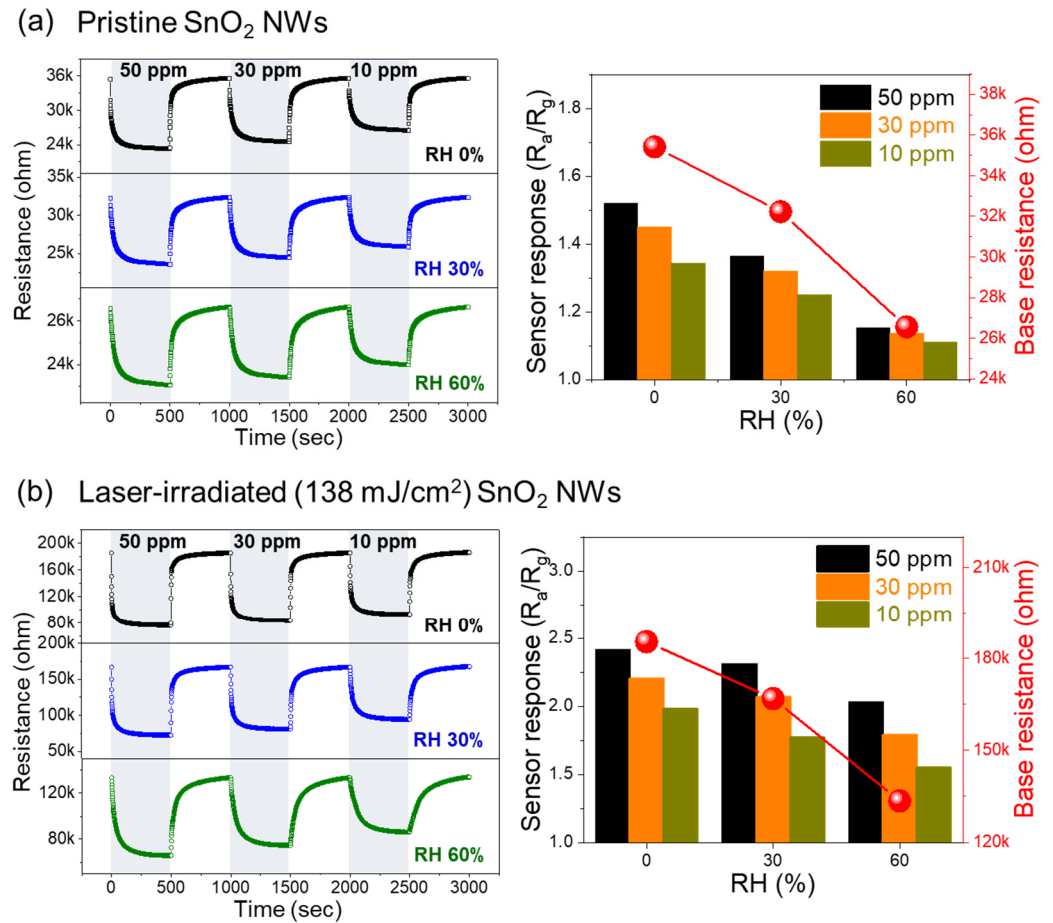
(a) Pristine SnO$_2$ NWs

(b) Laser-irradiated (138 mJ/cm^2) SnO$_2$ NWs

Figure 7. Dynamic resistance curves and corresponding sensor responses and base resistances at different RH levels for the (**a**) pristine and (**b**) laser-irradiated SnO$_2$ NWs with a laser energy density of 138 mJ/cm^2.

3.3. Gas-Sensing Mechanism

Oxygen molecules are adsorbed on the sensing materials (i.e., SnO$_2$ NWs) when the gas sensor is exposed to air, and the following reaction can occur because of the high electron affinity of oxygen [35,36]:

$$O_2(g) \rightarrow O_2(ads) \tag{2}$$

$$O_2(ads) + e^- \rightarrow O_2^- \tag{3}$$

$$O_2^- + e^- \rightarrow O^- \tag{4}$$

$$O^- + e^- \rightarrow O^{2-} \tag{5}$$

The adsorbed oxygen extracts electrons from the SnO$_2$ NW surface. Consequently, an electron depletion layer (EDL) is developed at the subsurface, and electrons are confined at the core of the SnO$_2$ NWs (known as the conduction volume or conduction channel). When a reducing target gas (C$_7$H$_8$ gas in this study) is supplied, the target gas adsorbs onto the SnO$_2$ NW surface instead of onto oxygen. Therefore, the electrons extracted from the oxygen return to the SnO$_2$ NWs, thus decreasing both the EDL width and sensor resistance. The relevant reactions are as follows [4,37]:

$$C_mH_n(g) \rightarrow C_mH_n(ads) \tag{6}$$

$$C_mH_n(ads) + xO^{-y}(ads) \rightarrow mCO_2 + n/2H_2O + xye^- \tag{7}$$
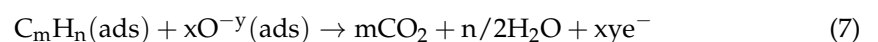
where, for toluene (C_7H_8) gas, "m" and "n" values are 7 and 8, respectively. x value is equal to $2m + n/2$; therefore, x value becomes 18 and y value is 1. As a result, the reaction is as follows:

$$C_7H_8(ads) + 18O^-(ads) \rightarrow 7CO_2 + 4H_2O + 18e^- \tag{8}$$
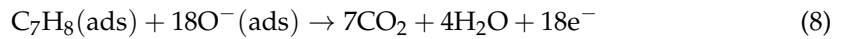
Next, we analyzed the mechanism of the improved sensor response after the FS laser was irradiated on the SnO_2 NWs. A higher initial sensor resistance facilitates better response by the chemosorbed gas sensor. This is because the sensor response is measured as R_a/R_g. For the laser-irradiated SnO_2-NW gas sensors, two different factors, i.e., the embossing surface and oxygen deficiency, should be considered. First, the FS laser irradiation creates an embossing surface on the SnO_2 NWs, as shown in the TEM image, which may increase the surface area of the SnO_2 NWs. Therefore, a greater amount of oxygen is adsorbed onto the SnO_2 NWs, thus increasing both the base resistance and gas response. Second, the FS laser irradiation results in oxygen deficiency in the SnO_2 NWs by forming SnO and SnO_x. This generates additional electron conduction, thus reducing both the base resistance and gas response. These two factors are conflicting; when the embossing surface effect is dominant, the sensor response is enhanced, whereas when the oxygen deficiency effect is dominant, the sensor response deteriorates. The sensor response was optimal at a laser energy density of 138 mJ/cm^2 but decreased as the laser energy density increased. This may be because the embossing surface effect was optimized at 138 mJ/cm^2, whereas the oxygen deficiency effect became more prominent as the laser energy density increased, which is attributed to a decrease in the sensor response. Figure 8 summarizes the sensing mechanism of the FS laser-irradiated gas sensor for C_7H_8 gas.
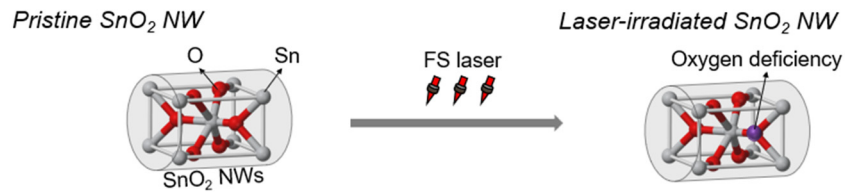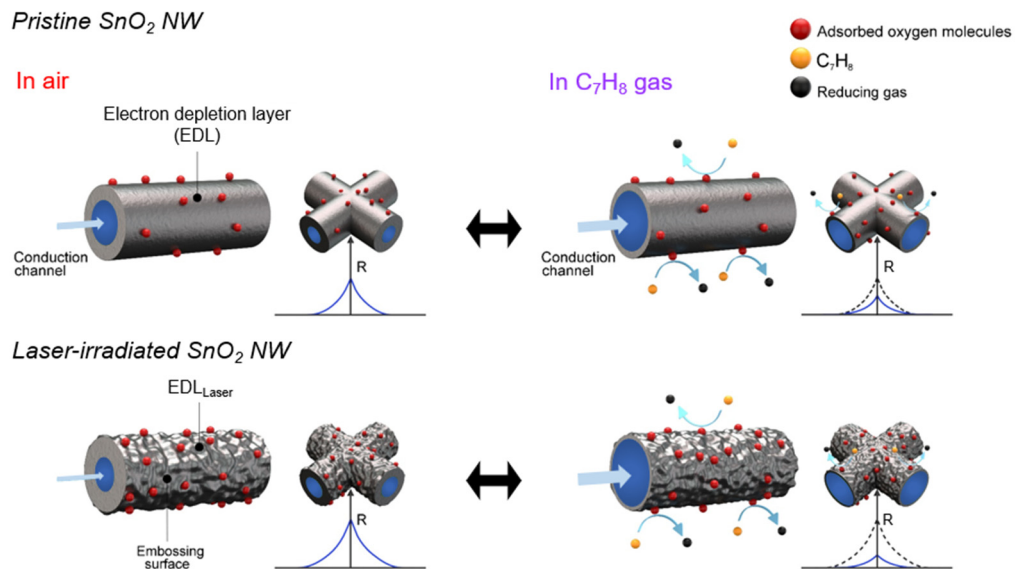

Figure 8. Schematic diagram of sensing mechanism of the laser-irradiated SnO_2 NWs in terms of oxygen vacancy and electron depletion.

3.4. Long-Term Stability Test

The fresh and 6-month-old SnO_2 gas sensor were used to examine the long-term stability of a laser-irradiated SnO_2-NW gas sensor. To the best knowledge of the authors, this is the first time the long-term stability of a laser-irradiated SnO_2-NW gas sensor has been investigated. Figure 9 shows the dynamic resistance curves and the corresponding sensor response for the pristine SnO_2 NWs (Figure 9a) and laser-irradiated SnO_2 NWs with a laser energy density of 138 mJ/cm^2 (Figure 9b) toward 0.6, 1, 10, 30, and 50 ppm of C_7H_8 gas. For the pristine and laser-irradiated SnO_2 NWs, the fresh and 6-month-old gas sensors showed comparable gas sensor performance. It is worth noting that the laser-irradiated SnO_2 NWs were able to sense 0.6 ppm of C_7H_8 gas with a sensor response of 1.06 and 1.07 for the fresh and 6-month-old sensors. On the contrary, no sensor response was examined at the C_7H_8 gas concentration of 0.6 ppm for the pristine SnO_2 NWs. This result supports the notion that FS laser irradiation enhances gas sensor sensitivity.
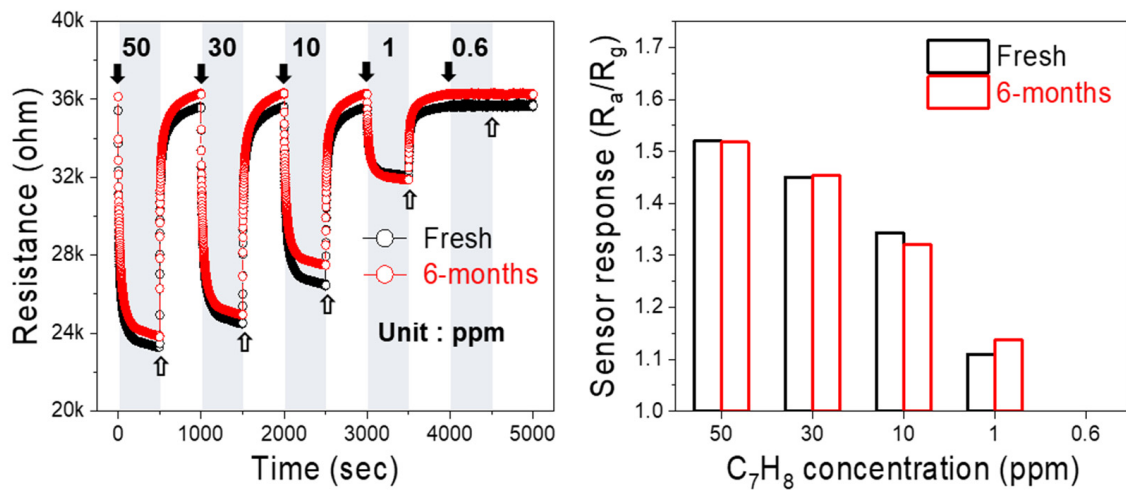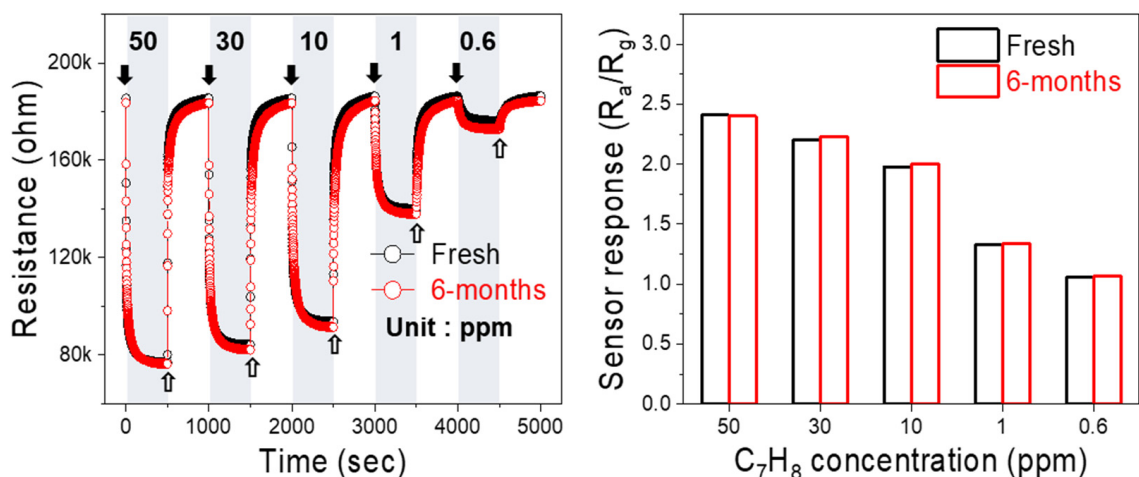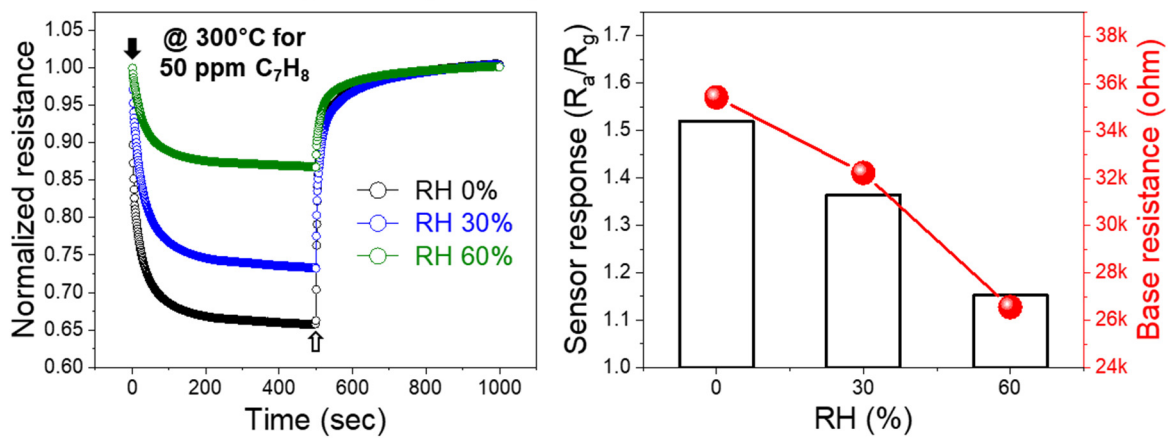

Figure 9. Dynamic resistance curves and corresponding sensor responses at different C_7H_8 gas concentrations for the fresh and 6-month-old gas sensors of (**a**) pristine and (**b**) laser-irradiated SnO_2 NWs with laser energy density of 138 mJ/cm^2.

Figure 10 compares the gas-sensing behavior at different RH levels for the fresh and 6-month-old gas sensors of pristine SnO_2 NWs and laser-irradiated SnO_2 NWs with a laser energy density of 138 mJ/cm^2. Figure 10a,b shows the normalized resistance curve and corresponding sensor response for the fresh and 6-month-old pristine SnO_2 gas sensors, respectively. Moreover, Figure 10c,d presents the normalized resistance curve and corresponding sensor response for the fresh and 6-month-old laser-irradiated SnO_2 gas sensors, respectively. The fresh and 6-month-old gas sensors show similar gas-sensing behaviors for both pristine and laser-irradiated SnO_2 NWs. Comparable sensor response values were obtained at different RH levels for the fresh and 6-month-old gas sensors of pristine SnO_2 NWs and laser-irradiated SnO_2 NWs. The long-term stability tests in Figures 9 and 10 indicate that no deterioration was detected in the sensing performance for both pristine and laser-irradiated SnO_2 NWs, even after 6 months from the gas sensor's fabrication. These results verify the robustness of laser-irradiated SnO_2-NW gas sensors.
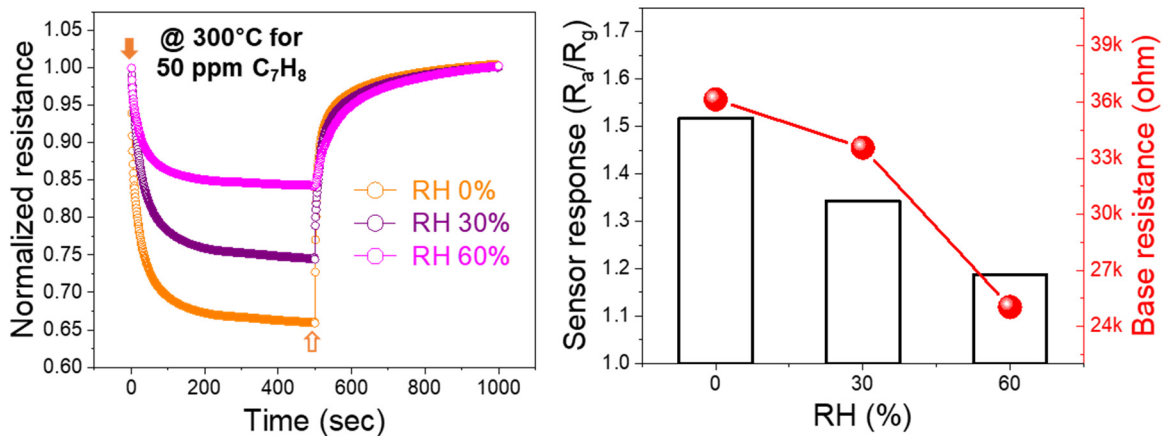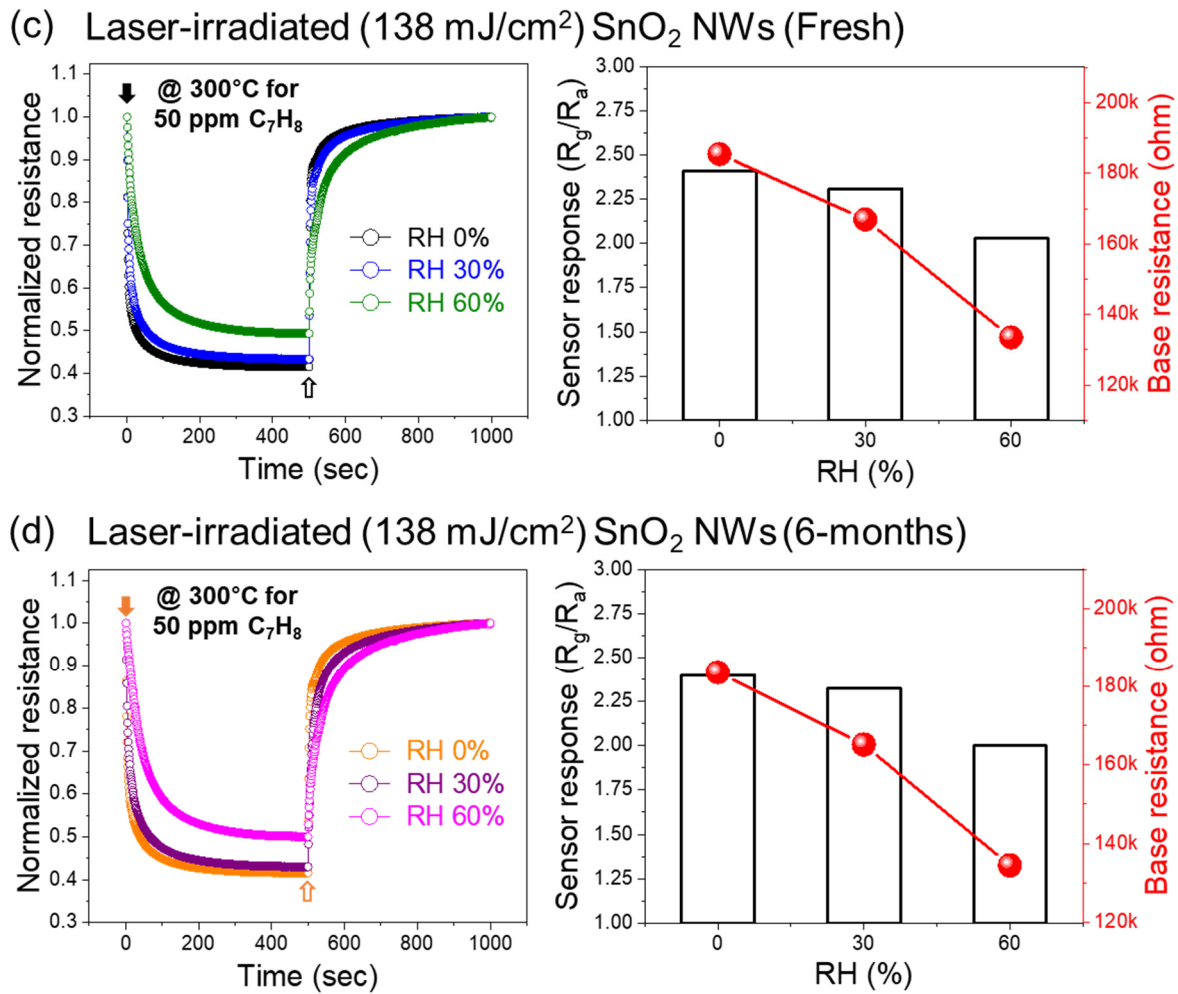

Figure 10. *Cont.*

Figure 10. Dynamic resistance curves and corresponding sensor responses at different RH levels for the (**a**) fresh and (**b**) 6-month-old gas sensors of the pristine SnO_2 NWs and the (**c**) fresh and (**d**) 6-month-old gas sensors of the laser-irradiated SnO_2 NWs with laser energy density of 138 mJ/cm^2.

4. Conclusions

In this study, the SnO_2 NWs were synthesized using the Au-catalyzed VLS method. Subsequently, the SnO_2 NWs were irradiated with the FS laser at energy densities of 138, 276, and 414 mJ/cm^2. Based on the results of the TEM analysis, the flat surface of the SnO_2 NWs transformed into an embossing surface with multiple nano-sized bumps owing to the FS laser irradiation. Moreover, the result of EELS analysis revealed that the FS laser irradiation induced the formation of the SnO and SnO_x phases in the SnO_2 NWs. Subsequently, the gas-sensing behavior toward C_7H_8 gas as a reducing gas was examined. The gas-sensing performance of the FS laser-irradiated SnO_2-NW gas sensor was superior to that of the pristine SnO_2-NW gas sensor. Specifically, the FS laser-irradiated gas sensor with a laser energy density of 138 mJ/cm^2 exhibited the highest gas response. The pristine SnO_2 NWs showed a sensor response level of 1.52 at 50 ppm of C_7H_8 gas, whereas the laser-irradiated SnO_2 NWs at 138 mJ/cm^2 showed a sensor response level of 2.42. The sensing mechanism of the laser-irradiated gas sensor was attributed to the formation of an embossing surface and the generation of oxygen deficiency at the SnO_2 NWs, which modulated the gas absorption sites and conduction channels, respectively. Moreover, the robustness of the laser-irradiated gas sensor was confirmed by verifying comparable gas-sensing behaviors between the fresh and 6-month-old gas sensors in different gas concentrations and RH levels.

Table 1 shows the sensitivity values of C_7H_8 gas with different SnO_2-based sensing materials. Compared with other studies, the FS laser-irradiated SnO_2 NWs showed a relatively low sensitivity value. However, those high sensitivity values were obtained with surface functionalization by using the heterojunction structure or catalytic effect. Different surface functionalization techniques or materials should be conducted to detect other target gases. Therefore, those approaches may have limited technological scalability. On the contrary, FS laser irradiation is a promising approach for enhancing the sensing performance toward multiple target gases because it is applicable to different types and shapes of SMOs.

Table 1. Comparison of SnO_2-based C_7H_8 gas sensing behavior.

Materials	Temperature (°C)	Concentration (ppm)	Response	References
Single SnO_2 nanowire	350	50	2.38	[27]
Pd-loaded SnO_2 cubic nanocages	230	20	41.4	[38]
SnO_2–ZnO core–shell nanowires	300	1	73	[39]
CuO-decorated spherical SnO_2	400	75	540	[40]
NiO–SnO_2 composite nanofiber	330	50	11	[41]
Au-coated SnO_2 nanorod	450	10	328	[42]
Pd-loaded flower-like SnO_2 microspheres	250	10	17.4	[43]

Author Contributions: Conceptualization, C.P.; investigation, S.A.; data curation, S.A. and K.W.C.; writing—original draft preparation, S.A. and K.W.C.; writing—review and editing, C.P.; supervision, C.P. All authors have read and agreed to the published version of the manuscript.

Institutional Review Board Statement: Not applicable.

Informed Consent Statement: Not applicable.

Data Availability Statement: Dataset available on request from the authors.

Conflicts of Interest: The authors declare no conflict of interest.

References

1. Timmer, B.; Olthuis, W.; van den Berg, A. Ammonia sensors and their applications—A review. *Sens. Actuators B* **2005**, *107*, 666–677. [CrossRef]
2. Hübert, T.; Boon-Brett, L.; Black, G.; Banach, U. Hydrogen sensors—A review. *Sens. Actuators B* **2011**, *157*, 329–352. [CrossRef]
3. Mirzaei, A.; Park, S.; Kheel, H.; Sun, G.-J.; Lee, S.; Lee, C. ZnO-capped nanorod gas sensors. *Ceram. Int.* **2016**, *42*, 6187–6197. [CrossRef]
4. Mirzaei, A.; Kim, J.-H.; Kim, H.W.; Kim, S.S. Resistive-based gas sensors for detection of benzene, toluene and xylene (BTX) gases: A review. *J. Mater. Chem. C* **2018**, *6*, 4342–4370. [CrossRef]
5. Kim, J.-H.; Lee, J.-H.; Mirzaei, A.; Kim, H.W.; Kim, S.S. Optimization and gas sensing mechanism of n-SnO_2-p-Co_3O_4 composite nanofibers. *Sens. Actuators B* **2017**, *248*, 500–511. [CrossRef]
6. Bang, J.H.; Choi, M.S.; Mirzaei, A.; Kwon, Y.J.; Kim, S.S.; Kim, T.W.; Kim, H.W. Selective NO_2 sensor based on Bi_2O_3 branched SnO_2 nanowires. *Sens. Actuators B* **2018**, *274*, 356–369. [CrossRef]
7. Choi, S.-W.; Jung, S.-H.; Kim, S.S. Significant enhancement of the NO_2 sensing capability in networked SnO_2 nanowires by Au nanoparticles synthesized via γ-ray radiolysis. *J. Hazard. Mater.* **2011**, *193*, 243–248. [CrossRef] [PubMed]
8. Kumar, V.; Sen, S.; Muthe, K.; Gaur, N.; Gupta, S.; Yakhmi, J. Copper doped SnO_2 nanowires as highly sensitive H_2S gas sensor. *Sens. Actuators B* **2009**, *138*, 587–590. [CrossRef]
9. Hu, P.; Du, G.; Zhou, W.; Cui, J.; Lin, J.; Liu, H.; Liu, D.; Wang, J.; Chen, S. Enhancement of ethanol vapor sensing of TiO_2 nanobelts by surface engineering. *ACS Appl. Mater. Interfaces* **2010**, *2*, 3263–3269. [CrossRef] [PubMed]
10. Ma, Y.; Qu, Y.; Zhou, W. Surface engineering of one-dimensional tin oxide nanostructures for chemical sensors. *Microchim. Acta* **2013**, *180*, 1181–1200. [CrossRef]

11. Kim, J.-H.; Mirzaei, A.; Kim, J.-Y.; Lee, J.-H.; Kim, H.W.; Hishita, S.; Kim, S.S. Enhancement of gas sensing by implantation of Sb-ions in SnO₂ nanowires. *Sens. Actuators B* **2020**, *304*, 127307. [CrossRef]

12. Pan, J.; Ganesan, R.; Shen, H.; Mathur, S. Plasma-modified SnO₂ nanowires for enhanced gas sensing. *J. Phys. Chem. C* **2010**, *114*, 8245–8250. [CrossRef]

13. Jiao, Z.; Wan, X.; Zhao, B.; Guo, H.; Liu, T.; Wu, M. Effects of electron beam irradiation on tin dioxide gas sensors. *Bull. Mater. Sci.* **2008**, *31*, 83–86. [CrossRef]

14. Kim, J.-H.; Mirzaei, A.; Kim, H.W.; Wu, P.; Kim, S.S. Design of supersensitive and selective ZnO-nanofiber-based sensors for H₂ gas sensing by electron-beam irradiation. *Sens. Actuators B* **2019**, *293*, 210–223. [CrossRef]

15. Lavanya, N.; Sekar, C.; Anithaa, A.; Sudhan, N.; Asokan, K.; Bonavita, A.; Leonardi, S.; Neri, G. Investigations on the effect of gamma-ray irradiation on the gas sensing properties of SnO₂ nanoparticles. *Nanotechnology* **2016**, *27*, 385502. [CrossRef] [PubMed]

16. Kim, J.-H.; Kim, J.-Y.; Lee, J.-H.; Mirzaei, A.; Kim, H.W.; Hishita, S.; Kim, S.S. Indium-implantation-induced enhancement of gas sensing behaviors of SnO₂ nanowires by the formation of homo-core–shell structure. *Sens. Actuators B* **2020**, *321*, 128475. [CrossRef]

17. Assar, M.; Karimzadeh, R. Enhancement of methane gas sensing characteristics of graphene oxide sensor by heat treatment and laser irradiation. *J. Colloid Interface Sci.* **2016**, *483*, 275–280. [CrossRef]

18. Hou, Y.; Jayatissa, A.H. Effect of laser irradiation on gas sensing properties of sol–gel derived nanocrystalline Al-doped ZnO thin films. *Thin Solid Films* **2014**, *562*, 585–591. [CrossRef]

19. Zhang, C.; Van Overschelde, O.; Boudiba, A.; Snyders, R.; Olivier, M.-G.; Debliquy, M. Improvement of sensing characteristics of radio-frequency sputtered tungsten oxide films through surface modification by laser irradiation. *Mater. Chem. Phys.* **2012**, *133*, 588–591. [CrossRef]

20. Al-Hashem, M.; Akbar, S.; Morris, P. Role of oxygen vacancies in nanostructured metal-oxide gas sensors: A review. *Sens. Actuators B* **2019**, *301*, 126845. [CrossRef]

21. Das, S.; Jayaraman, V. SnO₂: A comprehensive review on structures and gas sensors. *Prog. Mater. Sci.* **2014**, *66*, 112–255. [CrossRef]

22. Tomer, V.K.; Devi, S.; Malik, R.; Nehra, S.P.; Duhan, S. Highly sensitive and selective volatile organic amine (VOA) sensors using mesoporous WO₃–SnO₂ nanohybrids. *Sens. Actuators B Chem.* **2016**, *229*, 321–330. [CrossRef]

23. Ju, D.; Xu, H.; Xu, Q.; Gong, H.; Qiu, Z.; Guo, J.; Zhang, J.; Cao, B. High triethylamine-sensing properties of NiO/SnO₂ hollow sphere P–N heterojunction sensors. *Sens. Actuators B Chem.* **2015**, *215*, 39–44. [CrossRef]

24. Xu, Y.; Zheng, W.; Liu, X.; Zhang, L.; Zheng, L.; Yang, C.; Pinna, N.; Zhang, J. Platinum single atoms on tin oxide ultrathin films for extremely sensitive gas detection. *Mater. Horiz.* **2020**, *7*, 1519–1527. [CrossRef]

25. Xu, H.; Li, W.; Han, R.; Zhai, T.; Yu, H.; Chen, Z.; Wu, X.; Wang, J.; Cao, B. Enhanced triethylamine sensing properties by fabricating Au@SnO₂/α-Fe₂O₃ core-shell nanoneedles directly on alumina tubes. *Sens. Actuators B Chem.* **2018**, *262*, 70–78. [CrossRef]

26. Qiao, X.-Q.; Zhang, Z.-W.; Hou, D.-F.; Li, D.-S.; Liu, Y.; Lan, Y.-Q.; Zhang, J.; Feng, P.; Bu, X. Tunable MoS₂/SnO₂ P–N heterojunctions for an efficient trimethylamine gas sensor and 4-nitrophenol reduction catalyst. *ACS Sustain. Chem. Eng.* **2018**, *6*, 12375–12384. [CrossRef]

27. Tonezzer, M. Selective gas sensor based on one single SnO₂ nanowire. *Sens. Actuators B* **2019**, *288*, 53–59. [CrossRef]

28. Wang, B.; Zhu, L.F.; Yang, Y.H.; Xu, N.S.; Yang, G.W. Fabrication of a SnO₂ nanowire gas sensor and sensor performance for hydrogen. *J. Phys. Chem. C* **2008**, *112*, 6643–6647. [CrossRef]

29. Kuang, Q.; Lao, C.; Wang, Z.L.; Xie, Z.; Zheng, L. High-sensitivity humidity sensor based on a single SnO₂ nanowire. *J. Am. Chem. Soc.* **2007**, *129*, 6070–6071. [CrossRef] [PubMed]

30. Kim, J.-H.; Park, H.; Mirzaei, A.; Hahm, M.G.; Ahn, S.; Halik, M.; Park, C.; Kim, S.S. How femtosecond laser irradiation can affect the gas sensing behavior of SnO₂ nanowires toward reducing and oxidizing gases. *Sens. Actuators B Chem.* **2021**, *342*, 130036. [CrossRef]

31. Moreno, M.S.; Egerton, R.F.; Midgley, P.A. Differentiation of tin oxides using electron energy-loss spectroscopy. *Phys. Rev. B* **2004**, *69*, 233304. [CrossRef]

32. Jayababu, N.; Poloju, M.; Shruthi, J.; Reddy, M.R. Semi shield driven p-n heterostructures and their role in enhancing the room temperature ethanol gas sensing performance of NiO/SnO₂ nanocomposites. *Ceram. Int.* **2019**, *45*, 15134–15142. [CrossRef]

33. Wei, Y.; Zheng, H.; Hu, S.; Pu, S.; Peng, H.; Li, L.; Sheng, H.; Zhou, S.; Wang, J.; Jia, S. Controllable synthesis of single-crystal SnO₂ nanowires and tri-crystal SnO₂ nanobelts. *CrystEngComm* **2018**, *20*, 7114–7119. [CrossRef]

34. Kim, J.-H.; Mirzaei, A.; Kim, H.W.; Kim, S.S. Realization of Au-decorated WS₂ nanosheets as low power-consumption and selective gas sensors. *Sens. Actuators B* **2019**, *296*, 126659. [CrossRef]

35. Jian, Y.; Hu, W.; Zhao, Z.; Cheng, P.; Haick, H.; Yao, M.; Wu, W. Gas sensors based on chemi-resistive hybrid functional nanomaterials. *Nano-Micro Lett.* **2020**, *12*, 71. [CrossRef] [PubMed]

36. Gawali, S.R.; Patil, V.L.; Deonikar, V.G.; Patil, S.S.; Patil, D.R.; Patil, P.S.; Pant, J. Ce doped NiO nanoparticles as selective NO₂ gas sensor. *J. Phys. Chem. Solids* **2018**, *114*, 28–35. [CrossRef]

37. Hermawan, A.; Asakura, Y.; Inada, M.; Yin, S. One-step synthesis of micro-/mesoporous SnO₂ spheres by solvothermal method for toluene gas sensor. *Ceram. Int.* **2019**, *45*, 15435–15444. [CrossRef]

38. Qiao, L.; Bing, Y.; Wang, Y.; Yu, S.; Liang, Z.; Zeng, Y. Enhanced toluene sensing performances of Pd-loaded SnO₂ cubic nanocages with porous nanoparticle-assembled shells. *Sens. Actuators B* **2017**, *241*, 1121–1129. [CrossRef]

39. Kim, J.H.; Kim, S.S. Realization of ppb-Scale Toluene-Sensing Abilities with Pt-Functionalized SnO_2–ZnO Core–Shell Nanowires. *ACS Appl. Mater. Interfaces* **2015**, *7*, 17199–17208. [CrossRef] [PubMed]

40. Hermawan, A.; Asakura, Y.; Inada, M.; Yin, S. A facile method for preparation of uniformly decorated-spherical SnO_2 by CuO nanoparticles for highly responsive toluene detection at high temperature. *J. Mater. Sci. Technol.* **2020**, *51*, 119–129. [CrossRef]

41. Liu, L.; Zhang, Y.; Wang, G.; Li, S.; Wang, L.; Han, Y.; Jiang, X.; Wei, A. High toluene sensing properties of NiO–SnO_2 composite nanofiber sensors operating at 330 °C. *Sens. Actuators B* **2011**, *160*, 448–454. [CrossRef]

42. Lee, J.; Min, H.; Choe, Y.-S.; Lee, Y.G.; Kim, K.; Lee, H.-S.; Lee, W. Highly sensitive and selective detection of benzene, toluene, xylene, and formaldehyde using Au-coated SnO_2 nanorod arrays for indoor air quality monitoring. *Sens. Actuators B* **2023**, *394*, 134359. [CrossRef]

43. Tian, J.; Wang, J.; Hao, Y.; Du, H.; Li, X. Toluene sensing properties of porous Pd-loaded flower-like SnO_2 microspheres. *Sens. Actuators B* **2014**, *202*, 795–802. [CrossRef]